The very first normal-pressure tin borate $Sn_3B_4O_9$, and the intermediate $Sn_2[B_7O_{12}]F$†

Martin J. Schäfer,[a] Stephan G. Jantz,[a] Florian Pielnhofer[b] and Henning A. Höppe*[a]

Aside from amorphous phases, only a single crystalline tin borate had been synthesised so far under high pressure. In this work, we present the very first crystalline ternary tin borate $Sn_3B_4O_9$ synthesised under ambient pressure by decomposition of $Sn_3[B_3O_7]F$ above 500 °C. The crystal structure of $Sn_3B_4O_9$ ($P2_1/c$, Z = 4, a = 768.07(3) pm, b = 1206.78(4) pm, c = 924.96(3) pm, β = 101.847(1)°, 10 550 data, 147 parameters, R_1 = 0.028) determined by single-crystal X-ray diffraction comprises open layered borate polyanions with Sn(II) ions in-between showing the presence of a stereochemically active lone pair. $Sn_3B_4O_9$ was further characterized by DFT calculations and vibrational spectroscopy. Its optical band gap was calculated to approx. 3.5(1) eV. Tin borate was gained by thermal decomposition of $Sn[B_2O_3F_2]$ *via* a further new tin borate fluoride $Sn_2[B_7O_{12}]F$ ($C2/c$, Z = 8, a = 1037.99(2) pm, b = 859.78(2) pm, c = 2370.71(8) pm, β = 93.5650(10)°, 2674 data, 199 parameters, R_1 = 0.045).

Ternary borates are known of almost all main-group metals. In case of tin only a single crystalline high-pressure borate, *i.e.* β-SnB_4O_7 had been described so far by the Huppertz group.[1] Under ambient pressure normally glassy products are obtained. During our systematic investigation on silicate-analogous compounds like borosulfates[2,3] and fluorooxoborates,[4,5] we serendipitously discovered the very first ternary tin borate under normal pressure conditions, *i.e.* the title compound, as decomposition product of tin fluorooxoborate, *i.e.* $Sn[B_2O_3F_2]$ (in the cited literature named TFB).

Very recently, on our journey towards novel fluorooxoborates, we came across TFB comprising layers of condensed BO_3F tetrahedra and yielding an unique non-centrosymmetric crystal structure, almost simultaneously reported by Luo *et al.*[6]

During the investigation of the thermal decomposition of TFB we found two new phases, which to our impression, both are prerequisites for the formation of the first known crystalline tin borate under ambient pressure conditions, namely $Sn_3B_4O_9$ (**1**).

Heating TFB to 490 °C yields the first tin borate fluoride $Sn_3[B_3O_7]F$,[7] which itself decomposes around 520 °C to give **1**. Somewhat earlier, around 380 °C, we identified a further crystalline intermediate product as a large single-crystal in a differential scanning calorimetry crucible, the new tin borate fluoride $Sn_2[B_7O_{12}]F$ (**2**),[8] also published very recently.[9]

In this contribution we will elucidate the crystal structures of **1** and **2** as well as spectroscopic properties of **1**.

$Sn_3B_4O_9$ crystallises in a monoclinic unit cell (a = 768.07(3) pm, b = 1206.78(4) pm, c = 924.96(3) pm, β = 101.847(1)°) in space group $P2_1/c$ (no. 14) with four formula units per unit cell. It consists of Sn^{2+} cations embedded between borate polyanion layers. Their fundamental building block (FBB), a $B_4O_9^{6-}$ moiety, consists of one trigonal planar BO_3 triangle and three BO_4 tetrahedra, connected according to the descriptor 1△3□ : □<△□2> (Fig. 1, left).[10]

Two FBBs condense *via* the oxygen atoms O3 (Fig. 1, right) to dimers; these dimers connect further *via* O5 atoms to two-dimensional layers situated parallel to the (101) plane (Fig. 2).

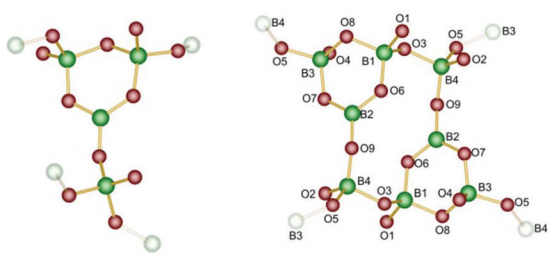

Fig. 1 Left: FBB of $Sn_3B_4O_9$, consisting of one trigonal-planar and three tetrahedral borate units; right: dimer of two FBBs with the respective atom labels; next neighbour boron atoms are faded, boron atoms green, oxygen atoms red.

[a]*Lehrstuhl für Festkörperchemie, Institut für Physik, Universität Augsburg, Universitätsstraße 1, D-86159 Augsburg, Germany.*
E-mail: henning.hoeppe@physik.uni-augsburg.de
[b]*Lehrstuhl für Anorganische Chemie, Universität Regensburg, Universitätsstraße 31, D-93053 Regensburg, Germany*

†Electronic supplementary information (ESI) available. See DOI: 10.1039/c9dt01901d

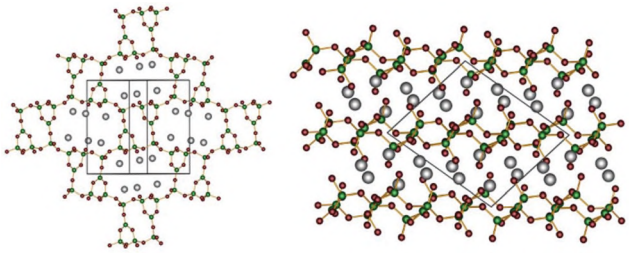

Fig. 2 Left: One layer of the polyanion, viewed along the <101> direction; Right: Layered structure of $Sn_3B_4O_9$ (tin atoms light grey, boron atoms green, oxygen atoms red).

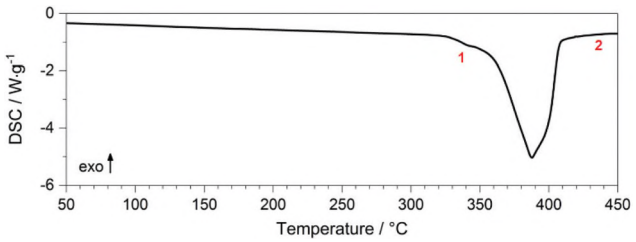

Fig. 4 DSC measurement representing the thermal decomposition of $Sn[B_2O_3F_2]$; at temperature **1**, the borate fluoride $Sn_2[B_7O_{12}]F$ is formed subject to decomposition further to the borate fluoride $Sn_3[B_3O_7]F$, which is present after the endothermic step (**2**)[10] which is an intermediate for the formation of $Sn_3B_4O_9$.

All three crystallographically different tin atoms are fivefold coordinated by terminal oxygen atoms showing the presence of a stereochemically active lone pair around Sn^{2+} as presented in Fig. 3.

Within the polyanion, the bond lengths agree well with the sums of the respective ionic radii.[11] All tetrahedral units show a very small deviation from tetrahedral symmetry as determined according to Balic-Žunic and Makovicky.[12,13] For the tetrahedral unit around B1 it was calculated to be 0.17%, 0.27% around B3 and 0.58% around B4. Thus, these can safely be classified as regular tetrahedra.

The three tin atoms in $Sn_3B_4O_9$ show a coordination environment that is strongly influenced by the lone pair of Sn^{2+} (Fig. 3). The angles inside the tripods are between 77 to 93° and the bond distances are ranging from 210.1 to 223.5 pm, agreeing well with the sum of their ionic radii.[14] Apart the tripod coordination, the tin atoms are coordinated by additional oxygen atoms that have larger interatomic distances (252 to 283 pm) and contribute very little to the coordination, according to our electrostatic calculations presented below.

$Sn_2[B_7O_{12}]F$ is an intermediate product that is formed within a very narrow temperature regime from $Sn[B_2O_3F_2]$ (Fig. 4). The DSC plot that led to a single crystal of $Sn_2[B_7O_{12}]F$ is displayed in Fig. S2 (in the ESI†).

$Sn_2[B_7O_{12}]F$ exhibits also a layered borate polyanion with tin atoms in-between and crystallises in space group $C2/c$ (no. 15) adopting a rather large unit cell with the cell parameters of a = 1037.99(2) pm, b = 859.78(2) pm, c = 2370.71(8) pm, β = 93.5650(10)° and Z = 8. The FBB of the polyanion (Fig. 5, left) consists of five trigonal planar BO_3 units and two BO_4 tetrahedra connected to form the hitherto unknown B_7O_{15} moiety obeying the descriptor 5△2□:△<□2△><2△□>. This reminds of the $B_7O_{15}^{3-}$ superstructural units in hydrated thallium borates,[15,16] but those are strictly no fundamental building units and also slightly different. These FBBs are connected *via* the oxygen atoms O15, O21 and O67 (Fig. 5) to two-dimensional layers parallel to (001). The Sn2 atoms are situated in the voids of these layers (Fig. 5, right), while the Sn1 atoms form $[SnF]^+$ dumbbells and are found between the anionic layers obeying a layer sequence of ABA′B′A. The distance of 206 pm between Sn1 and F1 corresponds to a covalent single bond, analogous to the $[SnF]^+$-units reported in $Sn_3[B_3O_7]F$.[10]

In addition to F1, Sn1 is coordinated by two oxygen atoms with the interatomic distances of 212–227 pm – forming the typical tripod coordination with angles of 73 to 86° – and a third significantly further distant oxygen atom with 254 pm. Sn2 is coordinated by a tripod (angles between 73 and 83°) out of F1 and two oxygen atoms with quite homogeneous distances between 227 and 235 pm as well as three further oxygen atoms with interatomic distances ranging between 253 pm and 298 pm.

According to electrostatic calculations presented below these oxygen atoms still contribute to the coordination of Sn2, although significantly weaker.

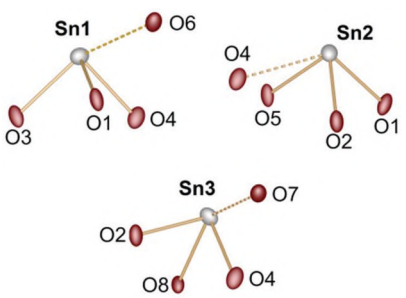

Fig. 3 Coordination environments of the three tin atoms in $Sn_3B_4O_9$. Atoms are shown as ellipsoids with 90% probability, tin atoms in light grey, oxygen atoms in red.

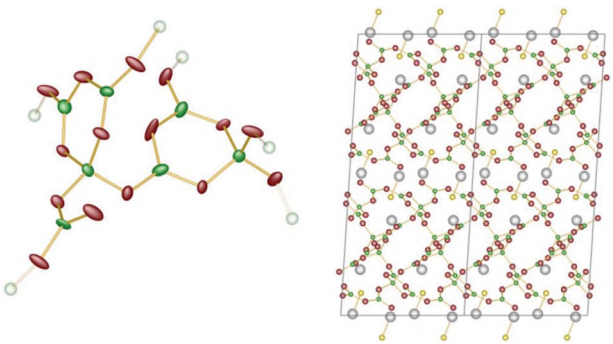

Fig. 5 Left: FBB of $Sn_2[B_7O_{12}]F$, the linking atoms O15, O21 and O67 are faded; Right: Crystal structure of $Sn_2[B_7O_{12}]F$, viewed along the <010> direction; tin atoms in light grey, boron atoms in green, oxygen atoms in red and fluorine atoms in yellow.

For both, $Sn_3B_4O_9$ and $Sn_2[B_7O_{12}]F$, we calculated the Madelung part of the lattice energy based on the MAPLE concept.[17,18] According to this method, the lattice energy of tertiary or quaternary compounds should equal the sum of binary compounds. For these calculations, we used 3 SnO[19] and 2 B_2O_3 [20] as base for $Sn_3B_4O_9$ and 7/2 B_2O_3, 1/2 SnF_2 [21] and 3/2 SnO[19] for $Sn_2[B_7O_{12}]F$.

Both compounds are electrostatically consistent, as their MAPLE values listed in Table 1 differ from the sum of MAPLE values of the binary compounds by less than 1%.

The electronic structure of $Sn_3B_4O_9$ was probed on different levels of theory. The band gap obtained with the generalized gradient approximation is 2.63 eV and extremely underestimates the experimental value. Stepping up the Jacobs ladder of density functionals to the range separated hybrids HSE06 and HSEsol results in more satisfying values (HSE06: 3.48 eV; HSEsol: 3.42 eV). All applied functionals describe the band gap to be of indirect nature which makes an experimental proof difficult. The valence band maximum (VBM) is located at the Γ point and the conduction band minimum (CBM) is at the Γ–Y line. There is also only a small discrepancy in energy between the global CBM at Γ–Y and a local minimum at the Γ-point making direct transitions conceivable (Fig. 6).

In the observed IR spectrum of $Sn_3B_4O_9$ (Fig. 7), all bands can be attributed to vibrations of the B–O bond, either in the trigonal-planar BO_3 or the tetrahedral BO_4 unit. A theoretical calculation of the vibrational frequencies gives further insight to the experimental recorded IR spectrum. Based on DFT calculations, the IR spectrum was simulated in order to attribute the observed peaks to specific modes. The complete simulated spectrum consists of 96 IR active vibrations. Around 1490 cm^{-1} the spectrum starts with symmetric stretching modes of the planar BO_3 units. With decreasing wavenumber the amount of symmetric BO_4 stretching modes and antisymmetric BO_3 stretching modes increases down to 720 cm^{-1}. Below 700 cm^{-1}, the stretching modes of the BO_3 and the BO_4 units mix up with bending vibrations. Modes in the range from 610 cm^{-1} to 400 cm^{-1} exclusively consist of bending vibrations, whereas bands below 550 cm^{-1} represent BO_4 bending only. Collective lattice vibrations cannot be observed in the experimental spectrum, those should arise below 400 cm^{-1}.

Table 1 Comparison of MAPLE energies for $Sn_3B_4O_9$ and $Sn_2[B_7O_{12}]F$

	$Sn_3B_4O_9$	$Sn_2[B_7O_{12}]F$
Calculated MAPLE/kJ mol^{-1}	55 652	83 999
Calculated MAPLE of the binary compounds/kJ mol^{-1}	55 242	83 960
Δ/%	0.74	0.04

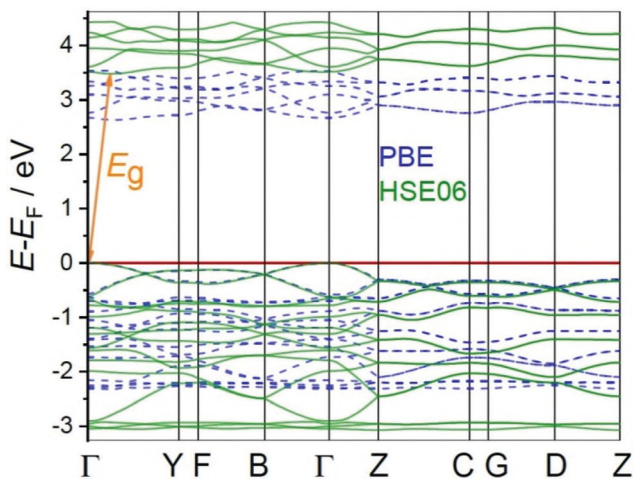

Fig. 6 Band structure of $Sn_3B_4O_9$ obtained with different functionals, showing the indirect band gap.

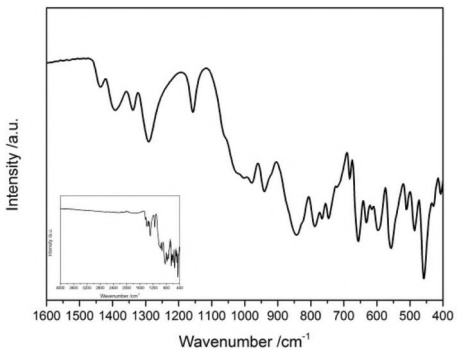

Fig. 7 Observed infrared spectrum of $Sn_3B_4O_9$. The inset shows the complete observed wavenumber range and that no water bands could be detected.

Synthesis of $Sn_3B_4O_9$

$Sn_3B_4O_9$ was synthesized in a two-step synthesis, starting from SnF_2 (Aldrich, 99%) and B_2O_3 (Alfa Aesar, 99.999%). Both starting materials were dried under vacuum at 150 °C and stored in a glovebox prior use. 499.8 mg (3.191 mmol) of SnF_2 and 222.1 mg (3.191 mmol) of B_2O_3 were carefully ground and filled into a monel crucible. The mixture was heated twice in an alumina tube furnace. First, the temperature was increased by 100 K h^{-1} to 490 °C, held at this temperature for 10 hours and then cooled to room temperature with 200 K h^{-1}. Afterwards the gained grey powder (phase pure $Sn_3[B_3O_7]F$) was ground. Employing the same heating rate the sample was maintained at 520 °C. The product, a light grey, non-hygroscopic and coarsely crystalline powder, consisted of $Sn_3B_4O_9$ with minor impurities of SnO_2; a powder diffraction pattern is presented in the ESI (Fig. S3†).

Synthesis of $Sn_2[B_7O_{12}]F$

$Sn_2[B_7O_{12}]F$ was synthesised in a aluminium DSC crucible, starting from $Sn[B_2O_3F_2]$.[4] The sample was heated to 380 °C

and cooled to 320 °C, then repeatedly heated and cooled down to the respective temperature for 18 additional cycles (see the DSC curve in Fig. S2 in the ESI†). One large crystal of $Sn_2[B_7O_{12}]F$ was obtained and one piece was broken off and characterised by single-crystal XRD.

X-ray structure determination

The X-ray data on which the structure solutions were based on were collected on a Bruker D8 Venture at room temperature, using Mo-K_α-radiation. All details on the measurements can be found in the ESI.† Further details of the crystal structures investigations may be obtained from the Fachinformationszentrum Karlsruhe, 76344 Eggenstein-Leopoldshafen, Germany (Fax: +49-7247-808-666; E-mail:crysdata@fiz-karlsruhe.de, http://www.fiz-karlsruhe.de/request for deposited data.html) on quoting the depository numbers CSD 1863601 ($Sn_2[B_7O_{12}]F$) and 1863602 ($Sn_3B_4O_9$).

IR Spectra were recorded on a Bruker EQUINOX 55 FT-IR-Spectrometer equipped with a Platinum ATR unit in the range 4000–400 cm^{-1} with a resolution of 4 cm^{-1} and 32 scans.

Quantum chemical calculations were performed in the framework of density functional theory (DFT) using a linear combination of Gaussian-type functions (LCGTF) scheme as implemented in CRYSTAL17[22,23] The total energy calculations including full structural optimisations were performed with the GGA (PBE)[24] xc-functional including Grimmes D3 dispersion correction.[25] Further the range separated hybrid functionals HSE06[26] and HSEsol[27] were used for the band structure calculations in order to obtain better agreement of experimental and calculated bandgaps. For the case of the hybrid functionals only experimental lattice parameters were used. The convergence criterion considering the energy was set to 1×10^{-8} a.u. with a k-mesh sampling of $6 \times 6 \times 6$. All-electron basis sets were taken from.[28–32] The vibrational frequencies were computed on the basis of the relaxed structures (PBE-D3), no imaginary frequencies were obtained hinting towards the optimization ended in an energetical minimum. Vibrational modes were visualized with the J-ICE application.[33] Further, a direct space analysis of the charge density was carried out by calculating the electron localization function (ELF) with TOPOND[34] interfaced to CRYSTAL17. 3D plots were visualized with XCrysDen.[35]

In this contribution we described the very first ternary tin borate obtained under ambient pressure conditions. Previous direct attempts to synthesise such compounds yielded glassy products. Under high pressure, a crystalline borate with higher density could be crystallised.[1] At normal pressure the apparent assistance by decomposition products containing fluoride seems compulsory as these presumably act as flux. During this detailed study we identified a further highly condensed tin borate fluoride as a large single crystal obtained directly in a DSC chamber as an intermediate product, which could not be reproduced by simple syntheses as its stability range covers only a few degrees centigrade.

Conflicts of interest

The authors declare no conflict of interest.

Acknowledgements

Support by the Deutsche Forschungsgemeinschaft (HO 4503/5-1) is gratefully acknowledged.

The authors also thank Prof. Bettina Lotsch, Dr. Ulrich Wedig, and the Computer Service group at the Max-Planck-Institute for Solid State Research (Stuttgart, Germany) for access to CRYSTAL17 and providing computational facilities.

Notes and references

1 J. S. Knyrim, F. M. Schappacher, R. Pöttgen, J. Schmedt auf der Günne, D. Johrendt and H. Huppertz, *Chem. Mater.*, 2007, **19**(2), 254.
2 P. Gross, A. Kirchhain and H. A. Höppe, *Angew. Chem., Int. Ed.*, 2016, **55**, 4353.
3 P. Netzsch, P. Gross, H. Takahashi and H. A. Höppe, *Inorg. Chem.*, 2018, **57**, 8530.
4 S. G. Jantz, M. Dialer, L. Bayarjargal, B. Winkler, L. van Wüllen, F. Pielnhofer, J. Brgoch, R. Weihrich and H. A. Höppe, *Adv. Opt. Mater.*, 2018, 1800497.
5 S. G. Jantz, F. Pielnhofer, L. van Wüllen, R. Weihrich, M. J. Schäfer and H. A. Höppe, *Chem. – Eur. J.*, 2018, **24**, 443.
6 M. Luo, F. Liang, Y. Song, D. Zhao, N. Ye and Z. Lin, *J. Am. Chem. Soc.*, 2018, **140**(22), 6814.
7 S. Schönegger, S. G. Jantz, A. Saxer, L. Bayarjargal, B. Winkler, F. Pielnhofer, H. A. Höppe and H. Huppertz, *Chem. – Eur. J.*, 2018, **24**, 1.
8 H. A. Höppe, S. G. Jantz, M. Dialer and M. Schäfer, presented at Hemdsärmelkolloquium at Leipzig, 2018.
9 Z. Lu, F. Zhang, A. Tudi, Z. Zhang, Z. Yang and S. Pan, *Inorg. Chem. Front.*, 2019, **4**, 996.
10 P. C. Burns, J. D. Grice and F. C. Hawthorne, *Can. Mineral.*, 1995, **33**, 1131.
11 R. D. Shannon, *Acta Crystallogr., Sect. A: Cryst. Phys., Diffr., Theor. Gen. Crystallogr.*, 1976, **32**, 751.
12 T. Balic-Žunic and E. Makovicky, *Acta Crystallogr., Sect. B: Struct. Sci.*, 1996, **52**, 78.
13 E. Makovicky and T. Balic-Žunic, *Acta Crystallogr., Sect. B: Struct. Sci.*, 1998, **54**, 766.
14 R. D. Shannon and C. T. Prewitt, *Acta Crystallogr., Sect. B: Struct. Crystallogr. Cryst. Chem.*, 1969, **25**, 925.
15 N. Penin, L. Segiun, B. Gérand, M. Touboul and G. Nowogrocki, *J. Solid State Chem.*, 2001, **160**, 139.
16 M. Touboul, C. Bois and D. Amoussou, *J. Solid State Chem.*, 1983, **48**, 412.
17 R. Hoppe, *Z. Naturforsch., A: Phys. Sci.*, 1995, **50**, 555.
18 R. Hübenthal, *MAPLE, Programm zur Berechnung des Madelunganteils der Gitterenergie, Vers. 4*, Universität Giessen, 1993.

19 J. Pannetier and G. Denes, *Acta Crystallogr., Sect. B: Struct. Crystallogr. Cryst. Chem.*, 1980, **36**, 2763.
20 G. E. Gurr, P. W. Montgomery, C. D. Knutson and B. T. Gorres, *Acta Crystallogr., Sect. B: Struct. Crystallogr. Cryst. Chem.*, 1970, **26**, 906.
21 R. C. McDonald, H. H. Hau and K. Eriks, *Inorg. Chem.*, 1976, **4**, 762.
22 R. Dovesi, A. Erba, R. Orlando, C. M. Zicowich-Wilson, B. Civalleri, L. Maschio, M. Rerat, S. Casassa, J. Baima, S. Salustro and B. Kirtman, *WIREs Comput. Mol. Sci.*, 2018, **8**, e1360.
23 R. Dovesi, V. R. Saunders, C. Roetti, R. Orlando, C. M. Zicowich-Wilson, F. Pascale, B. Civalleri, K. Doll, N. M. Harrison, I. J. Bush, P. D'Arco, M. Llunel, M. Causà, Y. Noël, L. Maschio, A. Erba, M. Rerat and S. Casassa, *CRYSTAL17 User's Manual*, University of Torino, Torino, 2017.
24 J. P. Perdew, K. Burke and M. Ernzerhof, *Phys. Rev. Lett.*, 1996, **77**, 3865.
25 S. Grimme, J. Anthony, S. Ehrlich and H. Krieg, *J. Chem. Phys.*, 2010, **132**(15), 15104.
26 J. Heyd, G. E. Scuseria and M. Ernzerhof, *J. Chem. Phys.*, 2003, **118**, 8207.
27 L. Schimka, J. Harl and G. Kresse, *J. Chem. Phys.*, 2011, **134**, 024116.
28 R. Orlando, R. Dovesi, C. Roetti and V. R. Saunders, *J. Phys.: Condens. Matter*, 1990, **2**, 7769.
29 J. Scaranto and S. Giogianni, *J. Mol. Struct.: THEOCHEM*, 2008, **858**, 72.
30 J. Rothballer, F. Bachhuber, S. M. Rommel, T. Söhnel and R. Weihrich, *RSC Adv.*, 2014, **4**, 42183.
31 F. Pielnhofer, F. Bachhuber, J. Rothballer, F. M. Schnappacher, R. Pöttgen and R. Weihrich, *Z. Anorg. Allg. Chem.*, 2014, **640**, 286.
32 J. Rothballer, F. Bachhuber, F. Pielnhofer, S. M. Schappacher, R. Pöttgen and R. Weihrich, *Eur. J. Inorg. Chem.*, 2013, 248.
33 P. Canepa, R. M. Hanson, P. Ugliengo and M. Alfredsson, *J. Appl. Crystallogr.*, 2014, **44**, 225.
34 C. Gatti and S. Cassassa, *Topond14* - http://www.crystal.unito.it/topond/topond.pdf, 2016.
35 A. Kokalj, *Comput. Mater. Sci.*, 2003, **28**, 155.